Editors' Suggestion

Tunable Josephson voltage source for quantum circuits

J.-L. Smirr,[1] P. Manset,[1] and Ç.Ö. Girit[1,2,*]

[1] *JEIP, UAR 3573, CNRS, Collège de France, PSL University, 11, place Marcelin Berthelot, 75005 Paris, France*
[2] *Quantronics Group, Université Paris Saclay, CEA, CNRS, SPEC, 91191 Gif-sur-Yvette, France*

(Received 30 December 2024; revised 16 July 2025; accepted 15 August 2025; published 3 November 2025)

Noisy voltage sources can be a limiting factor for both fundamental physics experiments and device applications in quantum information, mesoscopic circuits, magnetometry, and other fields. The best commercial dc voltage sources can be programmed to approximately six digits and have intrinsic noise in the microvolt range. On the other hand, the noise levels in metrological Josephson-junction-based voltage standards is subfemtovolt. Although such voltage standards can be considered "noiseless," they are generally not designed for continuous tuning of the output voltage nor for supplying current to a load at cryogenic temperatures. We propose a Josephson-effect-based voltage *source*, as opposed to a voltage standard, operating in the $30-160$-μV range, which can supply over 100 nA of current to loads at mK temperatures. We describe the operating principle, the sample design, and the calibration procedure to obtain continuous tunability. We show the current-voltage characteristics of the device, demonstrate how the voltage can be adjusted without dc control connections to room-temperature electronics, and showcase an experiment coupling the source to a mesoscopic load: a small Josephson junction. Finally, we characterize the performance of our source by measuring the voltage noise at the load, 50 pV rms, which is attributed to parasitic resistances in the cabling. This work establishes the use of the Josephson effect for voltage biasing of extremely sensitive quantum devices.

DOI: 10.1103/3xvr-ryh1

I. INTRODUCTION

Low-noise voltage sources are essential for sensitive electronics and basic science. The ultimate in voltage accuracy and precision is provided by quantum voltage standards based on the Josephson effect [1]. The parts-per-billion frequency stability of microwave oscillators combined with the ac Josephson relation, $V = (h/2e) \times f$, between voltage V and frequency f, have enabled a metrological definition of the volt [2]. Although Josephson standards are excellent for calibration or reference purposes [3], certain limitations have prevented their use as tunable voltage sources for precision applications in fields such as quantum information and mesoscopic physics. Most Josephson standards only provide a single fixed voltage in the range 1–10 V. The programmable Josephson voltage standard allows adjustment of the reference voltage, but only in discrete steps with undefined transient voltages during changes [4]. The Josephson arbitrary waveform synthesizer allows fine voltage resolution but requires complicated pulse-generation circuitry [5].

Here, we demonstrate a tunable, low-noise, metrologically accurate voltage source [6] that can operate continuously in the range 30–160 μV and which is simple to implement as it only requires a tunable microwave generator. This voltage range is suitable for applications such as Josephson spectroscopy [7], topological transconductance quantization [8], dc-pumped parametric amplification and squeezing [9,10], single microwave photon generation [11,12], entangled beam generation [13,14], and quantum thermodynamic engines [15].

The fundamental problem with using Shapiro steps for a tunable voltage source is that the steps are only stable for certain values of microwave power. In a Shapiro voltage *standard*, the amplitude of the microwave drive is precisely tuned at the working frequency to maximize the step height, thereby maintaining a stable output voltage. Continuously changing the voltage implies changing the working frequency; however, without simultaneous adjustment of the microwave amplitude, the voltage can switch to an arbitrary Shapiro step. By determining the optimal amplitude at each frequency, one can maintain a stable Shapiro step over a wide range of output voltage. This is the basic principle of the Josephson tunable voltage source.

*Contact author: caglar.girit@cnrs.fr

Published by the American Physical Society under the terms of the Creative Commons Attribution 4.0 International license. Further distribution of this work must maintain attribution to the author(s) and the published article's title, journal citation, and DOI.

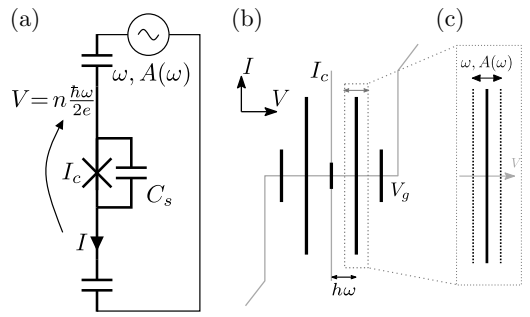


FIG. 1. (a) Circuit schematic of a Josephson tunnel junction driven by a microwave source showing locking to a Shapiro step at voltage $V = n\hbar\omega/2e$. Here, I_c is the junction critical current and C_s is a shunt capacitance. (b) Sketch of the current-voltage characteristic of the junction with (black) and without (light gray) microwave drive. When the drive amplitude is appropriately adjusted, Shapiro steps (thick vertical lines) appear. (c) After calibrating for the optimal microwave amplitude-frequency dependence $A(\omega)$ that maximizes the height of the first Shapiro step, the output voltage $V = \hbar\omega/2e$ can be continuously tuned without losing phase lock.

A schematic of the device is shown in Fig. 1(a). A Josephson tunnel junction of critical current I_c is capacitively coupled to a microwave voltage source of frequency ω and amplitude $A(\omega)$. The junction is shunted by a capacitance C_s, which lowers the plasma frequency, $\omega_p \approx \sqrt{2eI_c/\hbar C_s}$, allowing stable operation at lower voltages [16]. When the drive amplitude $A(\omega)$ is appropriately adjusted for the working frequency ω, the junction locks to the nth Shapiro step at voltage $V = n\hbar\omega/2e$.

The locking process can be understood from a sketch of the current-voltage (IV) characteristic of the Josephson tunnel junction, Fig. 1(b). Without a microwave drive, the IV characteristic (light gray) shows a supercurrent peak of amplitude I_c at zero voltage; a "subgap" region of zero average current for $0 < |V| < V_g$; and the quasiparticle branch for $|V| > V_g$, the superconducting gap voltage, where one recovers the normal-state resistance [17]. Under microwave drive, the IV characteristic shows Shapiro steps, vertical current peaks at voltages $V_n = n\hbar\omega/2e$ (thick black lines) [18]. When operated on a Shapiro step, the junction acts as a noiseless voltage source that can supply currents close to the maximum of the peak, $I_n(V_n)$.

Although the step position V_n depends solely on the microwave frequency and fundamental constants, the Shapiro step height depends on the microwave power at the junction, which varies with both the amplitude and frequency of the microwave source. Attenuation and imperfections in the transmission lines connecting the source to the junction, as well as an impedance mismatch at the junction, will influence the power delivered to the junction. Due to the Josephson nonlinearity [19], the effective junction impedance depends strongly on frequency and drive amplitude for $\omega \lesssim \omega_p$. At fixed frequency, the step height oscillates with microwave power, passing through zeros where phase locking of the voltage is not possible.

Because of the variability in coupled power with frequency, it is in general impossible to stay voltage locked while adjusting only the drive frequency. If the drive frequency falls on a value where the step height is zero, the voltage will switch to another step at different n, to the subgap region, or to the quasiparticle branch. To prevent unlocking, we propose a calibration procedure to determine the optimal power $A(\omega)$ to maximize the Shapiro step of a given order n. As shown in Fig. 1(c), by adjusting the microwave power according to $A(\omega)$, the Shapiro step height is maintained, and therefore the output voltage of the source can be tuned in a stable and continuous manner.

II. IMPLEMENTATION

An image of a microfabricated device is shown in Fig. 2(a), where the junction, capacitors, and pads have been colorized to match the circuit schematic in Fig. 2(b). The Josephson tunnel junction is made from aluminum using a Dolan-bridge technique and has a gap voltage of $V_g = 2\Delta/e = 400\,\mu\text{V}$. The shunt capacitor is a metal-insulator-metal structure with aluminum oxide dielectric and aluminum pads deposited by electron-beam evaporation. The plasma frequency of the capacitively shunted

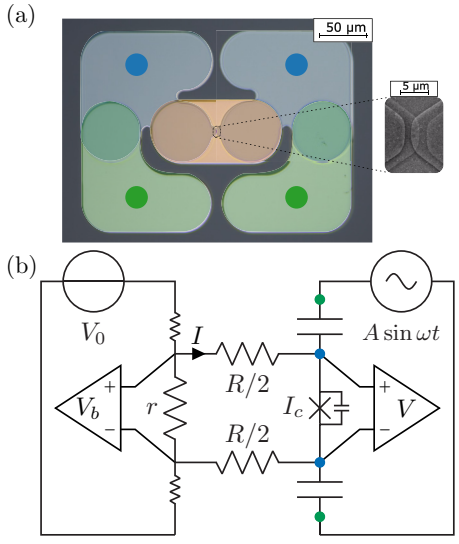


FIG. 2. (a) False-colored optical image of Josephson tunable voltage source and electron micrograph of the Josephson tunnel junction (inset). The shunt capacitor is highlighted in orange, and the bonding pads are highlighted in blue (dc connections) and green (microwave bias connection). (b) Circuit schematic for measurement of device current-voltage characteristic. An applied dc voltage V_0 induces the current $I = (V_b - V)/R$ through the junction. Here, V_b and V are measured with differential voltage amplifiers, and a microwave drive is applied via the signal generator $A\sin\omega t$.

junction is estimated to be $\omega_p = 6.8\,\text{GHz}$ and the inferred shunt capacitance is $C_s \approx 1.3\,\text{pF}$, which is consistent with the capacitor dimensions and dielectric constant. Electrical connections for the dc source (blue) and ac drive (green) are made via wirebonds to the indicated pads.

The device is loaded into a custom broadband microwave sample holder designed for operation up to 40 GHz and cooled in a dilution refrigerator with a base temperature of approximately 10 mK. All measurement lines are filtered to reduce electronic noise, and the microwave lines are attenuated to limit radiation from room temperature. The dc measurement and bias circuits are differential to reduce common-mode noise. Details of the experimental setup can be found in Appendix A.

Referring to the left-hand side of the schematic shown in Fig. 2(b), to measure the current-voltage (IV) characteristic, first, a voltage V_0 is applied to the dc bias line. The series combination of the resistors in the filtered bias line and a small shunt resistor $r \ll R$ located at the lowest-temperature stage of the cryostat forms a voltage divider. The attenuated dc voltage $V_b \ll V_0$ across the shunt resistor is measured with a low-noise room-temperature differential amplifier. A current I flows through the Josephson junction and two series resistors $R/2$. Another differential amplifier measures the dc voltage V across the junction, and the current I is calculated as $(V_b - V)/R$.

The right-hand side of Fig. 2(b) depicts a microwave drive $A \sin \omega t$ produced by a room-temperature signal generator. The microwaves are applied to the junction through microwave cabling and on-chip capacitors. Measurement of the IV characteristic of the junction consists of fixing A and ω, sweeping the dc bias V_0, and simultaneously measuring V_b and V to calculate I.

III. CALIBRATION

Figure 3(a) shows the IV characteristics as a function of microwave power at a fixed drive frequency $\omega_0/2\pi = 20\,\text{GHz}$. In the absence of microwave drive, $A = 0$, there is a single peak at zero voltage, the supercurrent peak (black trace). The mean switching current is 600 nA, close to the value of the current at the quasiparticle knee near the gap voltage $V_g = 400\,\mu\text{V}$, as expected by the Ambegaokar-Baratoff theory [7]. There are no Shapiro steps, and the subgap region is flat up to the gap voltage V_g. The bias voltage V_0 is swept upwards, and "switching" between the supercurrent peak and the subgap region is deduced from the dotted diagonal line near zero voltage. The slope of this load line is given by $1/(R + r)$.

Shapiro steps—current peaks in the subgap region—appear for nonzero drive amplitude $A > 0$ (colored traces). At an appropriate microwave drive strength, corresponding to a critical amplitude $A_1^{'c}$, the height of the first-order peak at $V = \hbar\omega_0/2e = 41.4\,\mu\text{V}$ is maximal and approximately 250 nA. Increasing the microwave amplitude to

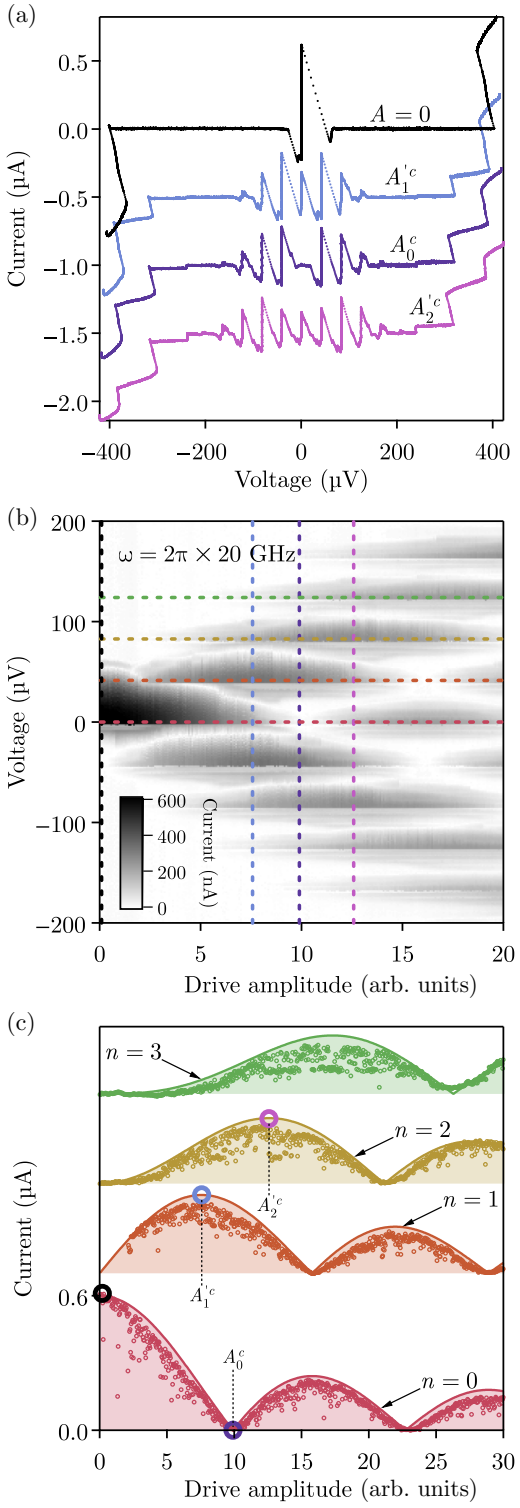


FIG. 3. (a) Current-voltage characteristics of Josephson tunable voltage source for different microwave drive amplitudes A at fixed frequency $\omega_0/2\pi = 20\,\text{GHz}$. Traces are offset by 0.5 μA for clarity. (b) Map of current as a function of microwave drive amplitude (x axis) and voltage (y axis), showing Shapiro step lobes. (c) Amplitudes of the supercurrent peak and first three Shapiro current steps, as extracted from the current-voltage map in (b), are plotted as a function of drive amplitude.

$A(\omega_0) = A_0^c$, the supercurrent peak ($n = 0$) vanishes, but steps of higher order persist. With stronger microwave drive, steps of higher order can be maximized, such as the second one ($A_2^{'c}$). In this notation, at drive amplitude $A_n^{'c}$, the nth current peak is at a maximum, whereas at A_n^c, the nth peak is at its first nontrivial zero.

In Fig. 3(b), the *IV* characteristics are plotted as a two-dimensional map over a broad range of microwave powers, with each pixel corresponding to the maximal absolute value of the measured current at a given bias voltage and drive amplitude. Shapiro steps appear as dark gray points grouped in horizontal line segments, with the contrast indicating the step height. The periodic, triangular pattern is expected from the Bessel-function dependence of step heights [16]. The *IV* traces of Fig. 3(a), measured at constant power, are indicated by vertical dashed lines.

The heights of steps $n = 0$–3, determined by taking the corresponding cuts of Fig. 3(b) (horizontal dashed arrows), are plotted as a function of microwave power in Fig. 3(c). They are fit to Bessel functions of the first kind, $|J_n|$, for orders $n = 0$–3. In contrast to Fig. 3(a), here, we see the continuous evolution of the step heights with $A(\omega)$: the supercurrent peak decreases and reaches its first zero (A_0^c) while the first- and second-order peaks reach their respective maxima at $A_1^{'c}$ and $A_2^{'c}$.

In principle, any of the critical points $A_0^c(\omega)$, $A_1^{'c}(\omega)$, or $A_2^{'c}(\omega)$ can be used to calibrate the incident power at the junction for frequencies $\omega \gtrsim \omega_p$, where the Bessel-function dependence is valid [16]. Junctions biased at lobe maxima, such as $A_1^{'c}(\omega)$ and $A_2^{'c}(\omega)$, serve as square-law power detectors, whereas junctions biased at zeros, such as $A_0^c(\omega)$, serve as linear detectors [20,21]. In addition to calibrating the microwave power using the Josephson effect, photon-assisted tunneling (PAT) of quasiparticles near the gap voltage can also be used for calibration [22].

For simplicity, we either use the first zero of the supercurrent, $A_0^c(\omega)$, or the PAT current to calibrate the power for a frequency range spanning approximately 8–40 GHz. Both of these techniques avoid complications arising from the hysteretic, nonlinear shape of the junction's *IV* characteristic. At each frequency, we determine the power necessary to either zero the supercurrent peak or to obtain a reference value of the PAT current near the quasiparticle knee. From the Bessel-function dependence of the critical point or the PAT current, we calculate the drive power necessary to maximize the Shapiro step of a given order. Technical details of the calibration procedure are given in Appendix B.

IV. PERFORMANCE

To demonstrate the quality of the calibration, Fig. 4(a) plots current-voltage characteristics with a microwave drive at 16, 18, and 20 GHz and amplitudes $A_0^c(\omega)$ corresponding to the first zero of the supercurrent. Shapiro steps up to order $n = 4$ are visible at multiples of voltages 33.09 μV for 16 GHz drive, 37.22 μV (18 GHz), and 41.36 μV (20 GHz), with a corresponding step spacing $n \times 2\,\text{GHz} \times h/2e \approx n \times 4.14\,\mu\text{V}$. As anticipated in the schematic, Fig. 1(c), the Shapiro step height within each order is approximately the same. A figure of merit μ for calibration is the ratio of the residual mean switching current, which should be zero for perfect calibration, to the maximum switching current, which is approximately 600 nA in the reference *IV* without microwave drive (black trace). The residual mean switching current for all three frequencies in Fig. 4(a) is less than 20 nA, giving $\mu \approx 3\%$.

Figure 4(b) shows a current-voltage map when driving at amplitude $A_0^c(\omega)$ over a wide frequency range. The measured average voltage is shown on the left-hand axis, the applied microwave drive frequency is on the bottom axis, and the maximum absolute value of the measured current is represented by the pixel contrast. The *IV* plots of Fig. 4(a) at 16, 18, and 20 GHz are indicated by color-coded dashed vertical lines. Colored arrows along the right-hand axis indicate Shapiro steps of order $n = -3$ to $n = 3$. Since the microwave drive is adjusted to $A_0^c(\omega)$, the supercurrent peak along the horizontal axis is virtually absent, and the nonzero orders are easily visible, although none is maximized.

From the current-voltage map, we numerically extract the mean switching current of the Shapiro steps and plot them as a function of frequency [Fig. 4(c)]. The residual supercurrent (black trace) is low, with $\mu \lesssim 10\%$ for almost the entire frequency range. In addition, the height of the first-order steps ($n = \pm 1$, blue traces) is more than 200 nA, or approximately a third of the zero-drive supercurrent, for a large range of frequencies. The Bessel-function dependence of step heights predicts that the first-order steps should be approximately 0.519 times the supercurrent peak for a microwave drive $A_0^c(\omega)$, and this appears to be the case in the frequency range 15–20 GHz, where the peak height reaches 300 nA. The measured step heights for the higher orders also agree with theory, as the expected peak-height ratios I_n/I_c for $n = 2$ and 3 are 0.432 and 0.2, respectively, compared to 1/3 ($n = \pm 2$, orange traces) and 1/6 ($n = \pm 3$, green traces) estimated from the data.

Some of the measured variation in the peak heights in Fig. 4(c) can be explained, such as the sharp drop above approximately 22 GHz, which is attributed to the deactivation of an attenuator, resulting in increased spurious noise, lowering switching currents. Discrepancies at lower frequencies may be due to weaker applicability of the Bessel-function form for step heights in that frequency range. Furthermore, microwave resonances on the chip or in the sample box may give rise to the narrow features superimposed on a generally smooth step-height dependence.

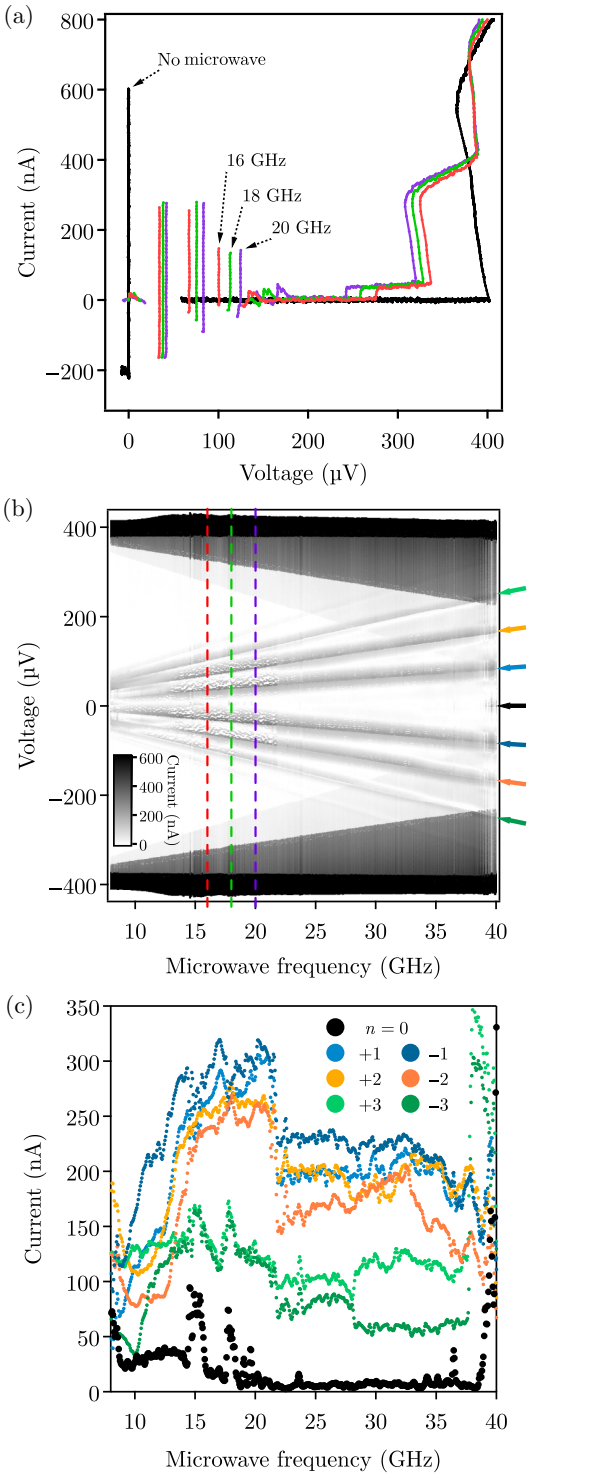


FIG. 4. (a) Current-voltage characteristics measured at optimal microwave amplitude $A_0^c(\omega)$ minimizing the supercurrent for $\omega/2\pi = 16$, 18, and 20 GHz. A reference *IV* without microwave drive is shown in black. Data are measured with a positive sweep in bias voltage, resulting in smaller negative peaks. (b) Current-voltage map measured at $A_0^c(\omega)$ plotted as a function of microwave drive frequency. The *IV* characteristics in (a) are indicated by vertical dashed lines. (c) Height of Shapiro peaks of order n extracted from (b) along the lines indicated by arrows.

To use the device as a tunable voltage source, it is crucial that the step amplitudes do not dip toward zero anywhere in the frequency range. Such dips will reduce the maximum possible source current and in the worst case, destroy phase lock. A load that sinks a current greater than the step amplitude will cause the source to switch off the Shapiro step. With our calibration procedure, it is possible to source at least 50 nA using any order over almost the entire frequency range, with the only exception being a narrow region near 10 GHz at $n = -3$.

V. STABILITY

Next, we consider the possibility of voltage locking without dc bias. Shapiro steps that cross at zero current—as shown in the sketch in Fig. 1(b) and demonstrated in the *IV* characteristic in Fig. 4(a)—may occur in underdamped Josephson junctions [23] and are used in zero-bias voltage standards [16,24]. A nonzero voltage-locked state is stable even in the absence of a bias current, and a voltage $n\hbar\omega/2e$ for $|n| > 1$ can spontaneously develop across a microwave-driven junction.

In Fig. 5, we show how the dc voltage on our junction can spontaneously lock to the drive frequency without any dc bias and then remain locked as the voltage is tuned continuously over a large range. For this purpose, we use a cryogenic switch to disconnect the dc bias V_0, shunt resistor r, and voltage probe V_b on the left-hand side of Fig. 2, breaking the current loop and forcing $I = 0$ (more details are given in Appendix A and Fig. 7); however, the junction voltage V can still be measured with dc connections to the voltage amplifier. To spontaneously switch to a Shapiro step, the phase must first unlock from the supercurrent branch at $n = 0$. To do so, the amplitude is ramped to the calibration point $A_0^c(\omega)$, where the effective supercurrent is zero. At this point, as a result of fluctuations, the voltage jumps to a Shapiro step of order n, which is typically ± 1. We then set the power to the calibration value $A_n^{'c}(\omega)$, which maximizes phase stability, subsequently adjusting it in tandem with the frequency.

We ramp the frequency up and down while locked to the first, $n = 1$, or second Shapiro step, $n = 2$, for a total duration of 100 min ($n = 1$) or 9 s ($n = 2$). The curve is continuous, and the voltage does not switch to zero or to another step.

VI. NOISE

To use the Josephson source in an experiment requiring a noiseless, tunable dc voltage, the device under test (DUT) should be connected to the source via a low-resistance, high-inductance interconnect, as shown in the circuit Fig. 6(a). Any parasitic resistance r_p between the source and the DUT should be as small as possible to limit thermal noise. The inductance L serves as an rf

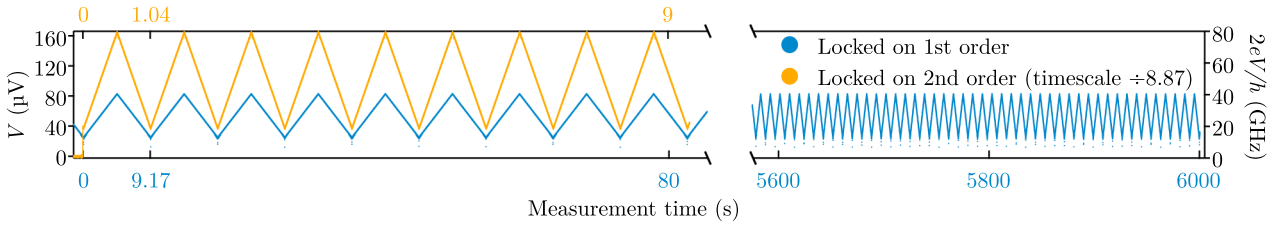


FIG. 5. After switching to the first Shapiro step (blue), the frequency is modulated in the range 10–40 GHz with a triangular waveform having a period of 9.17 s (bottom time scale). The power is adjusted according to the calibration to maintain the step amplitude. The measured junction voltage is continuous and follows the Josephson relation $V = \hbar\omega/2e$ without switching to other steps over a total time of 100 min. In orange, the junction is locked to the second-order step at $V = 2\hbar\omega/2e$, the sweep period is 1.036 s, and the measurement duration is approximately 9 s (top time scale). The biasing circuit is disconnected with a cryogenic switch during the measurement (see main text).

choke, blocking the microwave drive at ω_0 as well as harmonics $n\omega_0$ generated by the source. Ideally, the interconnection between the source and the DUT should be designed to avoid resonances at frequencies in the desired voltage range. The source and DUT can be located in the same enclosure, taking care to avoid microwave leakage between the source and DUT compartments, or in separate sample boxes.

As a proof-of-concept demonstration, we connect the source to a DUT, which is itself a small Josephson tunnel junction of critical current $I_e \approx 140\,\text{nA} \approx I_c/6$ [Fig. 6(a)]. The source and DUT are located in separate enclosures and connected by a superconducting twisted-pair cable (Fig. 7). Due to the ac Josephson effect, this "emitter" DUT converts the dc voltage from the source to a microwave signal. We couple the emitter via its on-chip capacitors to a cryogenic amplifier (see Fig. 8) and measure this signal using a microwave spectrum analyzer. Since the measured signal linewidth is proportional to the dc voltage noise at the emitter, we can characterize the residual voltage noise of our setup. The Josephson emission linewidth has been directly measured in this fashion for both large [25] and small junctions [26,27] biased with a conventional, noisy, dc voltage source. Effectively, the source junction down-converts a microwave drive to a dc voltage, which is then transmitted via low-frequency wiring to the emitter junction, which then up-converts the dc back to a microwave signal.

The microwave drive frequency is $\omega_0/2\pi = 7.69\,\text{GHz}$, and the amplitude has been chosen to maximize the step of order $n = 2$. The source junction is dc biased on the second Shapiro step at $V_2 = 2\hbar\omega_0/2e$. This allows differentiating the emitter Josephson frequency $2\omega_0$ from the drive frequency ω_0 of the source junction. Although the second harmonic of the microwave drive generated by the Josephson nonlinearity of the source junction is also at $2\omega_0 = 15.38\,\text{GHz}$, it is heavily attenuated by the cable connecting the source to emitter. This ensures that we measure the microwave signal resulting from down-conversion to dc and subsequent up-conversion by the emitter instead of direct frequency doubling by the source. We confirm that there is no harmonic leakage by checking that the microwave power output of the emitter at $2\omega_0$ is independent of the power incident on the source junction, provided that the source junction is locked on the second Shapiro step. A direct frequency-doubling process by the source junction would yield a Bessel-function dependence of the power detected at $2\omega_0$, whereas up-conversion from dc by the emitter yields a microwave current of amplitude bounded by I_e, independent of the incident power.

Figure 6(b) shows the spectrum measured at the cryostat base temperature. The full-width at half maximum (FWHM) of the Lorentzian peak is 37 kHz. The linewidth broadening, relative to that of the microwave source, can be explained by a small resistance r_p between the source and the emitter, indicated in the schematic of Fig. 6(a). The peak position $\omega_m/2\pi = (15.380\,012\,60 \pm 0.000\,000\,02)\,\text{GHz}$ is detuned from $2\omega_0$ by $\Delta\omega = 2\omega_0 - \omega_m \approx 2\pi \times 12.6\,\text{kHz}$. This detuning can result from a parasitic dc current i_p flowing through the resistance r_p, which gives a voltage drop $i_p r_p = \hbar\Delta\omega/2e = V_2 - \tilde{V}_2$. The origin of this dc current is likely to be inelastic Cooper-pair tunneling [28,29], in which the microwave power generated by the emitter and absorbed in its environment is balanced by the dc power supplied by the source.

We obtain $r_p \approx 20 - 30\,\text{m}\Omega$ using three different methods: equating r_p with the known contact resistance of the connectors (30 mΩ); using $r_p = \hbar\Delta\omega/2ei_p$ with i_p estimated as the inelastic Cooper-pair current arising from a 50-Ω microwave environment (20 mΩ); and extracting r_p from the slope of the detuned voltage $\tilde{V}_2$ as a function of a current bias applied to the source (24 mΩ).

With zero series resistance between the source and the emitter, we would expect a much narrower linewidth than the measured value, 37 kHz. The emission linewidth is broadened by thermal fluctuations in the resistor r_p, which have a voltage-noise density $4k_B T r_p$, where k_B is Boltzmann's constant and T is the electronic temperature. For a Lorentzian lineshape, the expected FWHM is $4\pi k_B T r_p (2e/h)^2$, assuming a rectangular power spectrum

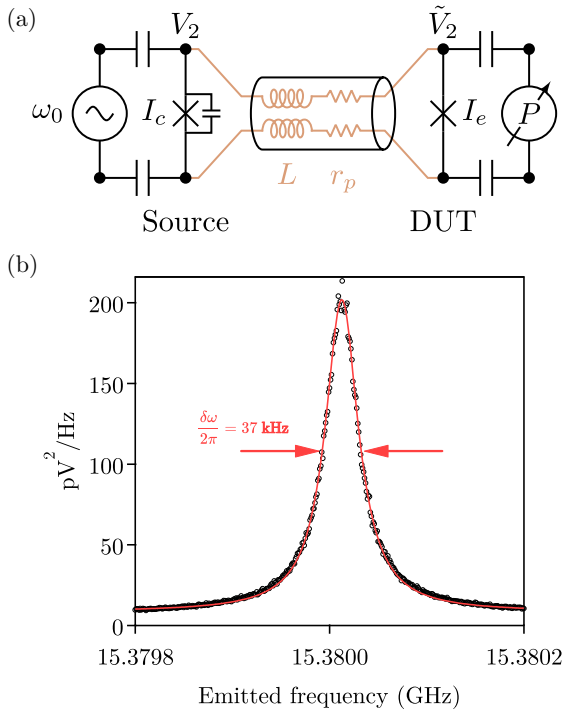


FIG. 6. (a) A small Josephson junction (critical current $I_e < I_c$), serving as a device under test (DUT, right), is coupled to the Josephson voltage source via a superconducting twisted-pair cable of inductance L and small parasitic resistance r_p. The source and DUT are located in separate sample boxes (Fig. 7). A microwave drive of frequency $\omega_0/2\pi = 7.690$ GHz is applied to switch the junction to the second Shapiro step at voltage $V_2 = 2\hbar\omega_0/2e = 31.80\,\mu$V. The dc voltage at the DUT, $\tilde{V}_2 \approx V_2$, is converted by the Josephson effect to a microwave signal of frequency $\omega_m \approx 2\omega_0$, which is measured with a spectrum analyzer (symbol P) after amplification (not shown, see Fig. 8). (b) The power spectrum shows a narrow peak at $\omega_m/2\pi = (15.380\,012\,60 \pm 0.000\,000\,02)$ GHz with a FWHM linewidth of 37 kHz (red fit).

for the noise [26,30]. This result is independent of the cutoff frequency, which could be thermal, k_BT/h, or given by $1/r_pC$ for sufficiently large r_pC, where C is the effective capacitance of the cables and wiring in parallel with the emitter junction.

Using $r_p = 25\,\text{m}\Omega$, the emission linewidth is compatible with a reasonable electronic temperature, $T = 36\,\text{mK}$. Reducing the linewidth to sub-kHz levels would require care to eliminate parasitic resistance between the source and the DUT. Every milliohm of resistance at a low electronic temperature of 25 mK contributes 1 kHz to the linewidth. When the source and the DUT are separated by superconducting wires, the resistance of connector pins, which dominates in this case, as well as solder and printed-circuit-trace resistances must be minimized. Despite the inadvertent parasitic resistance, the measured frequency precision is 2.4 ppm. The inferred low-frequency voltage-noise density at the emitter junction is approximately 220 fV/$\sqrt{\text{Hz}}$, and the total rms voltage noise is less than 50 pV.

VII. CONCLUSION

We have demonstrated a tunable, low-noise voltage source based on the ac Josephson effect, operating in the range 30–160 μV and capable of delivering 100 nA of current, making it well suited to loads in the kΩ range. The calibration procedure optimizes stability of the voltage output across a wide frequency range, and the source maintains phase lock without an applied dc bias for an indefinite period. One can connect to the voltage source with low-frequency superconducting wires or interconnects, taking care to minimize parasitic resistances, but it is not necessary to have the source and the load in the same enclosure. In practice, the dc connection used to monitor the output voltage can be eliminated given the metrological relationship of source voltage to microwave drive frequency. In addition to continuous tunability, the source has low noise and metrological accuracy.

Future work could extend the upper voltage limit, possibly using series arrays of Josephson junctions or employing different junction materials such as niobium. To achieve lower operating voltages, one would need to increase the shunt capacitance, which reduces the plasma frequency and lowers the minimum voltage for stable Shapiro steps [16]. A more complex microwave drive, such as biharmonic or pulsed, could allow deterministic switching to specific Shapiro steps. The current range could be extended using larger junctions or parallel arrays.

Our proof-of-concept experiment coupling the source to a small Josephson junction demonstrates the possibility of integrating ultralow-noise, tunable, cryogenic dc voltage bias into devices for quantum information, quantum sensing, and mesoscopic physics. Specific applications include microwave photon emitters [13,26], Josephson spectroscopy [7,31], dc-pumped parametric amplification [10,32,33], and qubit stabilization [34].

ACKNOWLEDGMENTS

We thank V. Benzoni, J. Griesmar, L. Peyruchat, J.-D. Pillet, and F. Lafont for discussions and assistance with the experiments. We thank Fabien Portier and Ambroise Peugeot for critical feedback. This project has received funding from the European Research Council (ERC) under the European Union's Horizon 2020 research and innovation program (Grant Agreement No. 636744). The research was also supported by IDEX Grant No. ANR-10-IDEX-0001-02 PSL, a Paris "Programme Emergence(s)" Grant, and the CNRS "Prématuration" program.

DATA AVAILABILITY

The data that support the findings of this article are openly available [35].

APPENDIX A: EXPERIMENTAL DETAILS

The experiments were conducted in a Bluefors LD250 dilution refrigerator with a base temperature below 10 mK. A photograph and a complete simplified circuit can be found in Fig. 7.

The source IV characteristics are obtained by sweeping V_b with the double-pole, double-throw (DPDT) electromechanical switch Sw closed (KEMET EC2-12SNU) [36]. The voltage V is measured, and the current I is calculated using $I = (V - V_b)/R$, where $R = 80\,\Omega$ is the sum of two series thin-film resistors. Thermal and instrument noise is filtered as shown in Fig. 8, where the colors match those in Fig. 7(b).

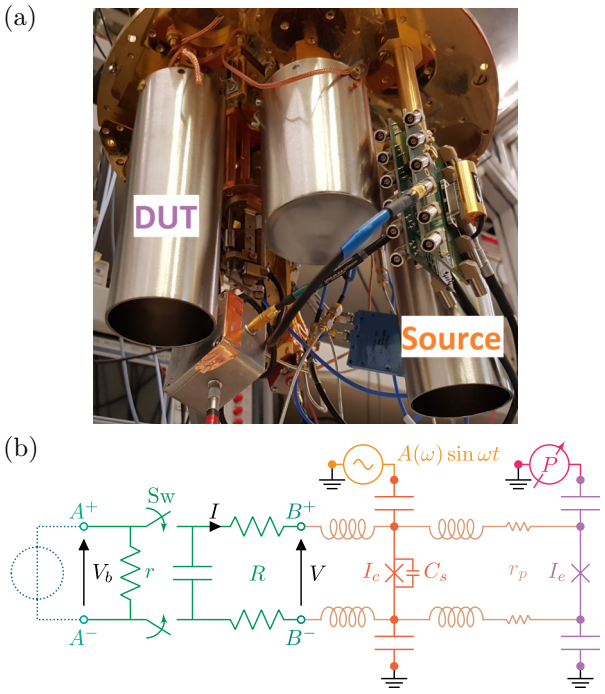


FIG. 7. (a) Photograph of the source (right) and DUT (left) in their magnetically shielded sample holders attached to the dilution refrigerator. The source, the DUT, and a biasing circuit box (not visible) are connected to each other by NbTi twisted pairs terminated by LEMO.00.302 connectors (not visible). Some elements appear on the photograph that are not related to the experiment described in this article. (b) Schematic of the source (orange) connected to the emitter (purple) with biasing circuit (green) via NbTi twisted pairs (brown). Details of ac bias (gold) and measured ac power (pink) are available in Fig. 8, as well as details of dc supply (blue) and differential measurement of V_b and V (probe points indicated by circles $A^{\pm}$ and $B^{\pm}$). The DPDT electromechanical relay (Sw) allows the supply to be disconnected and the current shunt to be broken.

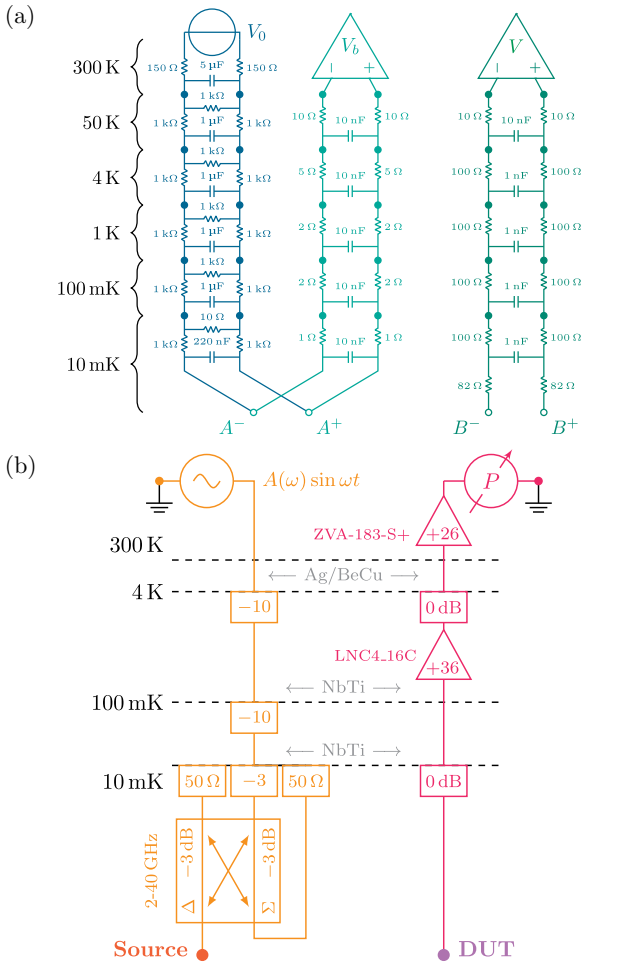


FIG. 8. Details of the cryostat wiring: (a) the dc wiring comprises twisted pairs equipped with filtering RC circuits thermally anchored at all temperature stages of the cryostat; (b) the ac wiring uses standard copper coaxial cables with 2.92 mm connectors, except NbTi between 10 mK and 4 K and silver-plated BeCu from 4 K to room temperature. The 1- and 50-K stages are bypassed in ac.

All connections are made with balanced, differential twisted pairs. The 20-Ω bias resistor r has a large volume to thermalize electrons. A room-temperature floating voltage source supplies a voltage V_0, which is attenuated ($\sim 1/25000$) and RC filtered to produce the bias voltage V_b. Both V_b and V are measured using low-noise differential preamplifiers (NF LI-75).

During zero-bias operation, the supply can be disconnected by toggling Sw using a ± 0.3 V, 0.1 s long pulse delivered via a superconducting twisted pair (not depicted). A bypass capacitor, together with resistors R, filters unwanted transients.

The bias, source, and emitter are interconnected by NbTi twisted pairs about 30-cm long, providing inductance to attenuate high frequencies while having zero dc resistance. The residual parasitic resistance r_p discussed in the main

text is attributed to the pins of the connectors in the cable between the source and the DUT (LEMO 0.5 mm pins).

On the ac end of the source, the microwave drive is applied via coaxial cables with distributed attenuators totaling 23 dB. The 2–40-GHz hybrid coupler adds 3 dB attenuation but terminates the sample with a 50-Ω load at 10 mK while dumping low-frequency noise to another 50-Ω load.

On the ac end of the emitter, the spectrum is measured with a signal analyzer (Rohde&Schwarz FSVA30) after cryogenic (LNF LNC4_16C) and room-temperature (Mini-Circuits ZVA-183-S+) amplification. Two "0-dB" XMA attenuators help with cable thermalization. No other filtering is used.

The sample is mounted on a printed circuit board (PCB) covered by a copper lid used as a mechanical and thermal anchor to the mixing chamber of the cryostat [Fig. 9]. To minimize the effect of electromagnetic cavity resonances, the sample box is designed to be small, and an Eccosorb absorber is affixed to the lid. Filtering capacitors are added to damp electrical modes in wirebonds and the PCB. The sample is magnetically shielded by the combination of an inner aluminum cylinder and an outer cylinder made of Cryophy, a high-magnetic-permeability material that is compatible with low temperatures. The PCB includes sockets for a differential dc connector (LEMO 00.302) and a microwave connector (2.92 mm).

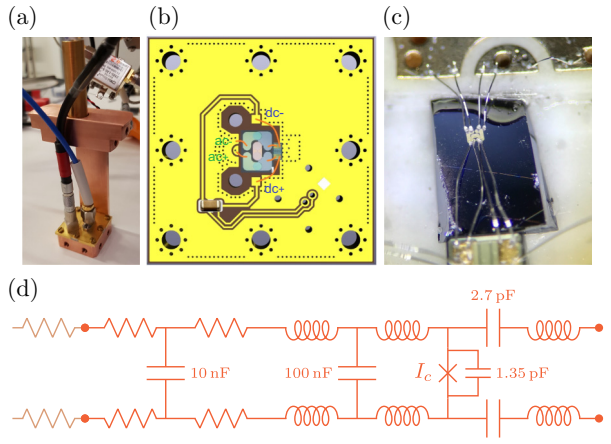


FIG. 9. (a) Photo of the sample holder used for both the source and the emitter. Sample holders are housed in cylindrical shields visible in Fig. 7(a). (b) Drawing of the PCB and wirebonds to the source sample, with 100-nF silicon and 10-nF ceramic filtering capacitors. (c) Close-up photo of the sample wirebonded to the 2.92-mm PCB launch and the 100-nF silicon filtering capacitor. Wirebonds to dc pads are partially visible. (d) Electrical schematic of the source chip and PCB. The emitter schematic is identical, but the 1.35-pF on-chip shunt capacitor C_s is absent. The inductors represent Al wirebonds, and the resistors represent the nonsuperconducting elements, including cable connector (brown), socket, and PCB tracks, which comprise the parasitic resistance r_p.

The Dolan-type aluminum Josephson junction, shunt capacitor, and microwave coupling capacitor are fabricated using optical lithography and electron-beam evaporation. The bottom electrodes of the capacitors are deposited in the same step as the junction, followed by alumina evaporation constituting the first 30 nm of the insulators. The rest of the alumina insulation (60 nm) and the top electrodes (aluminum, 200 nm) are deposited after a second round of lithography. Electrical connection to the junction at the bottom-electrode level is made via wirebonds that break through the insulating layers.

APPENDIX B: CALIBRATION

In the main text, we discuss two methods for calibrating the microwave power, i.e., obtaining values $A_n'^c(\omega)$ of the drive amplitude that maximize a given nth-order Shapiro step at different frequencies. Calibrating at discrete values ω_i separated by 10 to 100 MHz is sufficient, and intermediate frequencies can be obtained by interpolation.

The photon-assisted tunneling (PAT) method consists in choosing a reference PAT current I^* and finding the microwave drive amplitude $A^*(\omega_i)$ at which this PAT current is obtained for a given frequency ω_i. In practice, we bias the junction around a voltage V just below the superconducting gap, set a microwave frequency ω_i and amplitude A, and modulate it at a low rate f (typically 10–100 Hz). Then, we proceed to a lock-in measurement of the current I at frequency f. This enables measurement of low PAT currents, where $I \propto A$. With such a linear relationship, it is straightforward to implement a software feedback loop that converges to the value A^* corresponding to the reference PAT current I^*. Calibration data $A_n'^c(\omega_i)$ are obtained by correcting values $A^*(\omega_i)$ by a constant factor that depends on chosen step n and reference PAT current I^*. A limitation of this method is that V should be adjusted with ω because the PAT current has a stepped distribution that shifts with drive frequency. Furthermore, it is difficult to reliably set V at lower drive frequencies because of the hysteresis in the IV characteristic near the superconducting gap; however, because the PAT current is monotonic with A, it is a reliable method for moderate-accuracy calibration.

A more accurate calibration method uses the suppression of the supercurrent I_0 with drive power. The approximate position of the first zero of $I_0 = I_c J_0(A)$ is determined using the PAT calibration method. For each drive frequency ω_i, the amplitude A is swept around the position of the predicted zero. We record the amplitude $A_0^c(\omega_i)$ at which the junction switches to nonzero voltage. This constitutes the calibrated reference from which, using the properties of Bessel functions, we calculate $A_n'^c(\omega_i)$, the amplitude that maximizes the Shapiro peak of order n. Experimentally, the supercurrent suppression is detected

by measuring V while applying (via V_b) a small bias current $I = I_b \ll I_c$: when supercurrent is reduced to $I_0 \lesssim I_b$, the junction switches from zero-voltage to a finite voltage RI_b. Here, I_b is chosen to be as small as permitted by the signal-to-noise ratio of V.

[1] B. Jeanneret and S. P. Benz, Application of the Josephson effect in electrical metrology, Eur. Phys. J. Spec. Top. **172**, 181 (2009).

[2] P. J. Mohr and B. N. Taylor, CODATA recommended values of the fundamental physical constants: 2002, Rev. Mod. Phys. **77**, 107 (2002).

[3] A. Rüfenacht, N. E. Flowers-Jacobs, and S. P. Benz, Impact of the latest generation of Josephson voltage standards in ac and dc electric metrology, Metrologia **55**, S152 (2018).

[4] C. J. Burroughs, P. D. Dresselhaus, A. Rufenacht, D. Olaya, M. M. Elsbury, Y.-H. Tang, and S. P. Benz, NIST 10 V programmable Josephson voltage standard system, IEEE Trans. Instrum. Meas. **60**, 2482 (2011).

[5] S. P. Benz and C. A. Hamilton, A pulse-driven programmable Josephson voltage standard, Appl. Phys. Lett. **68**, 3171 (1996).

[6] C. Girit and J.-L. Smirr, Voltage source and method for calibrating this voltage source (2023), FR patent FR3114171B1, US patent US20230341880A1 pend.

[7] J. Griesmar, R. H. Rodriguez, V. Benzoni, J.-D. Pillet, J.-L. Smirr, F. Lafont, and Ç. Ö. Girit, Superconducting on-chip spectrometer for mesoscopic quantum systems, Phys. Rev. Res. **3**, 043078 (2021).

[8] L. Peyruchat, J. Griesmar, J.-D. Pillet, and Ç. Ö. Girit, Transconductance quantization in a topological Josephson tunnel junction circuit, Phys. Rev. Res. **3**, 013289 (2021).

[9] S. Jebari, F. Blanchet, A. Grimm, D. Hazra, R. Albert, P. Joyez, D. Vion, D. Estève, F. Portier, and M. Hofheinz, Near-quantum-limited amplification from inelastic Cooper-pair tunnelling, Nat. Electron. **1**, 223 (2018).

[10] U. C. Mendes, S. Jezouin, P. Joyez, B. Reulet, A. Blais, F. Portier, C. Mora, and C. Altimiras, Parametric amplification and squeezing with an ac- and dc-voltage biased superconducting junction, Phys. Rev. Appl. **11**, 034035 (2019).

[11] A. Grimm, F. Blanchet, R. Albert, J. Leppäkangas, S. Jebari, D. Hazra, F. Gustavo, J.-L. Thomassin, E. Dupont-Ferrier, F. Portier, and M. Hofheinz, Bright on-demand source of antibunched microwave photons based on inelastic Cooper pair tunneling, Phys. Rev. X **9**, 021016 (2019).

[12] C. Rolland, A. Peugeot, S. Dambach, M. Westig, B. Kubala, Y. Mukharsky, C. Altimiras, H. le Sueur, P. Joyez, D. Vion, P. Roche, D. Esteve, J. Ankerhold, and F. Portier, Antibunched photons emitted by a dc-biased Josephson junction, Phys. Rev. Lett. **122**, 186804 (2019).

[13] A. Peugeot, G. Ménard, S. Dambach, M. Westig, B. Kubala, Y. Mukharsky, C. Altimiras, P. Joyez, D. Vion, P. Roche, D. Esteve, P. Milman, J. Leppäkangas, G. Johansson, M. Hofheinz, J. Ankerhold, and F. Portier, Generating two continuous entangled microwave beams using a dc-biased Josephson junction, Phys. Rev. X **11**, 031008 (2021).

[14] S.-l. Ma, X.-K. Li, Y.-L. Ren, J.-K. Xie, and F.-L. Li, Antibunched n-photon bundles emitted by a Josephson photonic device, Phys. Rev. Res. **3**, 043020 (2021).

[15] N. Lörch, C. Bruder, N. Brunner, and P. P. Hofer, Optimal work extraction from quantum states by photo-assisted Cooper pair tunneling, Quantum Sci. Technol. **3**, 035014 (2018).

[16] R. L. Kautz, Noise, chaos, and the Josephson voltage standard, Rep. Prog. Phys. **59**, 935 (1996).

[17] T. Orlando and K. A. Delin, *Foundations of Applied Superconductivity* (Addison-Wesley, Reading, Mass., 1991).

[18] S. Shapiro, A. R. Janus, and S. Holly, Effect of microwaves on Josephson currents in superconducting tunneling, Rev. Mod. Phys. **36**, 223 (1964).

[19] K. K. Likharev, *Dynamics of Josephson Junctions and Circuits* (CRC Press, Boca Raton, FL, 1986).

[20] P. Richards, F. Auracher, and T. Van Duzer, Millimeter and submillimeter wave detection and mixing with superconducting weak links, Proc. IEEE **61**, 36 (1973).

[21] J. Zmuidzinas and P. Richards, Superconducting detectors and mixers for millimeter and submillimeter astrophysics, Proc. IEEE **92**, 1597 (2004).

[22] J. R. Tucker and M. J. Feldman, Quantum detection at millimeter wavelengths, Rev. Mod. Phys. **57**, 1055 (1985).

[23] M. T. Levinsen, R. Y. Chiao, M. J. Feldman, and B. A. Tucker, An inverse ac Josephson effect voltage standard, Appl. Phys. Lett. **31**, 776 (1977).

[24] R. L. Kautz, On a proposed Josephson-effect voltage standard at zero current bias, Appl. Phys. Lett. **36**, 386 (1980).

[25] I. Yanson, V. Svistunov, and I. Dmitrenko, Experimental observation of the tunnel effect for Cooper pairs with the emission of photons, Sov. Phys. JETP **21**, 650 (1965).

[26] M. Hofheinz, F. Portier, Q. Baudouin, P. Joyez, D. Vion, P. Bertet, P. Roche, and D. Esteve, Bright side of the Coulomb blockade, Phys. Rev. Lett. **106**, 217005 (2011).

[27] M. C. Cassidy, A. Bruno, S. Rubbert, M. Irfan, J. Kammhuber, R. N. Schouten, A. R. Akhmerov, and L. P. Kouwenhoven, Demonstration of an ac Josephson junction laser, Science **355**, 939 (2017).

[28] G.-L. Ingold and Y. V. Nazarov, in *Single Charge Tunneling: Coulomb Blockade Phenomena In Nanostructures* (Springer US, Boston, MA, 1992), Chap. 2, pp. 21–107.

[29] T. Holst, D. Esteve, C. Urbina, and M. H. Devoret, Effect of a transmission line resonator on a small capacitance tunnel junction, Phys. Rev. Lett. **73**, 3455 (1994).

[30] J. L. Stewart, The power spectrum of a carrier frequency modulated by Gaussian noise, Proc. IRE **42**, 1539 (1954).

[31] A. Peugeot, H. Riechert, S. Annabi, L. Balembois, M. Villiers, E. Flurin, J. Griesmar, E. Arrighi, J.-D. Pillet, and L. Bretheau, Two-tone spectroscopy of high-frequency quantum circuits with a Josephson emitter, Phys. Rev. Appl. **22**, 064027 (2024).

[32] R. Albert, J. Griesmar, F. Blanchet, U. Martel, N. Bourlet, and M. Hofheinz, Microwave photon-number amplification, Phys. Rev. X **14**, 011011 (2024).

[33] U. Martel, R. Albert, F. Blanchet, J. Griesmar, G. Ouellet, H. Therrien, N. Nehra, N. Bourlet, A. Peugeot, and

M. Hofheinz, Influence of bias-voltage noise on the inelastic Cooper-pair tunneling amplifier (ICTA), Appl. Phys. Lett. **126**, 074001 (2025).

[34] L. Danner, F. Höhe, C. Padurariu, J. Ankerhold, and B. Kubala, Quantum microwaves: Stabilizing squeezed light by phase locking, Phys. Rev. B **111**, 184519 (2025).

[35] J.-L. Smirr, P. Manset, and Ç. Ö. Girit, Figure data for current article, https://doi.org/10.5281/zenodo.14577236 (2024).

[36] N. Beev and M. Kiviranta, Note: Cryogenic low-noise dc-coupled wideband differential amplifier based on SiGe heterojunction bipolar transistors, Rev. Sci. Instrum. **83**, 066107 (2012).